A Significantly Twisted Spirocyclic Phosphine Oxide as a Universal Host for High-Efficiency Full-Color Thermally Activated Delayed Fluorescence Diodes

Jing Li, Dongxue Ding, Youtian Tao, Ying Wei, Runfeng Chen, Linghai Xie, Wei Huang, and Hui Xu**

Thermally activated delayed fluorescence (TADF) materials and diodes have emerged in recent years.[1] Most TADF emitters are pure organic compounds, featuring donor–acceptor (D–A) systems with near-zero singlet–triplet splitting (ΔE_{ST}).[2] TADF dyes can utilize triplet exciton through the efficient reverse intersystem crossing from triplet (T_1) to singlet (S_1) excited states for 100% theoretically internal quantum efficiency (η_{int}).[3] However, similar to phosphorescent organic light-emitting diodes (PHOLEDs), the involvement of long-lifetime triplet excitons amplifies the influence of collision-induced quenching effects, including triplet–triplet annihilation (TTA), singlet–triplet annihilation (STA), and triplet–polaron quenching, on device performance.[4] Consequently, TADF dyes are commonly dispersed in host matrixes to mitigate intermolecular interactions, which substantially promotes the device efficiencies.[5] However, different to PHOLEDs using heavy-metal complex emitters, the dopants and hosts in the emissive layers (EMLs) of TADF diodes are both pure organic compounds with similar components and optical properties. In this case, not only dopant–dopant but also host–dopant interactions would worsen exciton quenching,[6] making the hosts dominant in quenching suppression, besides their functions in carrier injection/transportation and energy transfer.[7]

J. Li, D. Ding, Dr. Y. Wei, Prof. H. Xu
Key Laboratory of Functional
Inorganic Material Chemistry
Ministry of Education and School of
Chemistry and Material Science
Heilongjiang University
74 Xuefu Road, Harbin 150080, China
E-mail: hxu@hlju.edu.cn, iamhxu@njtech.edu.cn
Prof. Y. Tao, Dr. Y. Wei, Prof. W. Huang, Prof. H. Xu
Key Laboratory of Flexible Electronics (KLOFE)
and Institute of Advanced Materials (IAM)
Jiangsu National Synergetic Innovation Center
for Advanced Materials (SICAM)
Nanjing Tech University (NanjingTech)
30 South Puzhu Road, Nanjing 211816, China
E-mail: wei-huang@njtech.edu.cn
Prof. R. Chen, Prof. L. Xie, Prof. W. Huang
Key Laboratory for Organic Electronics
and Information Displays (KLOEID)
Institute of Advanced Materials (IAM)
Nanjing University of Posts and Telecommunications
9 Wenyuan Road, Nanjing 210023, China

DOI: 10.1002/adma.201506286

With an increasing requirement on device performance, especially efficiency stability, in recent years, much attention has been paid to TADF host material development with a focus on molecular engineering pertinent to structural and optoelectronic characteristics of specific TADF dyes.[8] The state-of-the-art external quantum efficiencies (EQE) (η_{ext}) of monocolor and white hybrid diodes were achieved as ≈15% for yellow and red, ≈20% for green and blue, and ≈15% for white, approaching to the current levels of PHOLEDs. Nevertheless, the further improvement of the device performance is limited by the small number of high-efficacy TADF materials available currently. Noticeably, recent studies about universal phosphorescent host materials have already manifested the superiority of utilizing a single host for multicolor devices with favorable efficiencies,[9] which is another main drawback of TADF host development because none of the host materials reported so far are generally suitable to full-color TADF devices. Universal host materials have the superiority in fabrication simplification and production cost saving, since display pixels with different colors can be produced with similar and even the same configurations, and multiple EMLs of lighting devices can be integrated. The absence of universal TADF host materials should be attributed to the various molecular polarities and configurations of TADF dyes with different emission colors, which give rise to diverse intermolecular interactions and exciton quenching channels. With respect to the essence of quenching effects as collision induction,[10] the challenge for developing universal TADF hosts is embodied in extremely rigorous demand on suppressing dopant–dopant and host–dopant interactions.

Spirocyclic structures with two orthogonal conjugated rigid planes are widely employed in organic semiconductors for various optoelectronic applications,[11] by virtue of their steric hindrance. Nevertheless, the orthogonal symmetry of spirocyclic structures is still favorable for intermolecular ordered packing and π–π interactions. In this sense, twisted and asymmetrical spiro compounds with remarkably reduced intermolecular interactions can be regarded as a feasible alternative as universal hosts for full-color TADF diodes. Our group developed a series of spiro[fluorene-9,9′-xanthene] (SFX)-based organic semiconductors for electroluminescence (EL).[12] The xanthene ring in SFX is relatively flexible for distortion, providing an additional space for further configuration optimization. In this contribution, on the basis of a short-axis linkage strategy, we designed and prepared a highly twisted and asymmetrical SFX phosphine oxide host substituted with a single diphenylphosphine oxide (DPPO) group at its 4′-position (**Figure 1**a). By

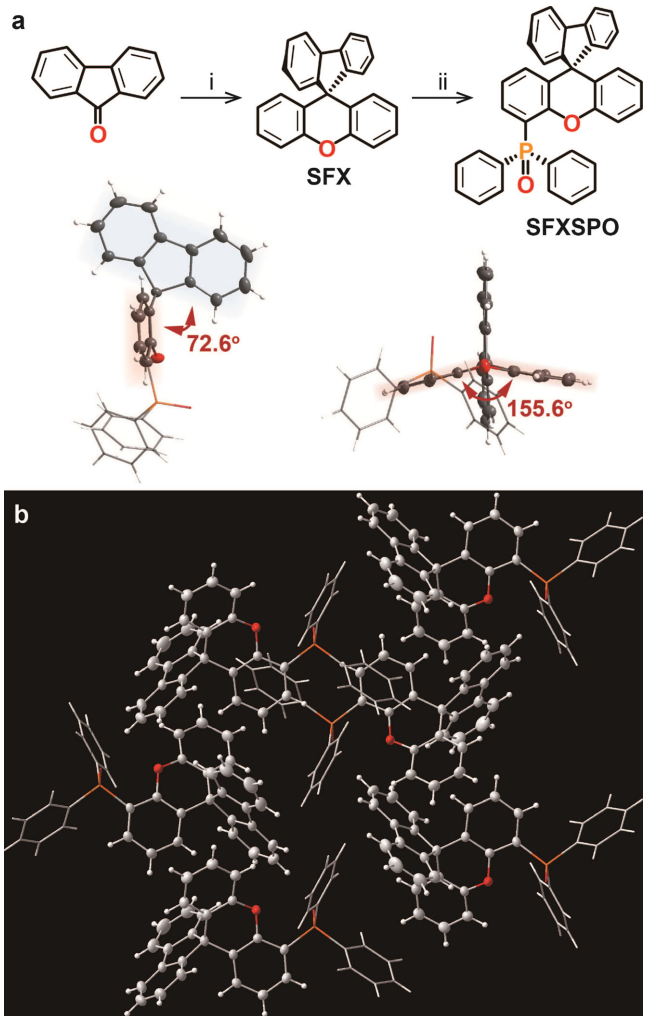

Figure 1. a) Synthetic procedure of SFXSPO: i) Phenol, CF_3SO_3H, 80 °C; ii) *n*-BuLi, Ph_2PCl, THF, −78 °C to room temperature, 30% H_2O_2, and lateral and bottom views of single crystal structure for SFXSPO; b) packing diagram of single crystal for SFXSPO.

virtue of its nonplanar xanthene and oblique fluorene, 4′-diphenylphosphinoylspiro[fluorene-9,9′-xanthene] (SFXSPO) realizes highly disordered molecular packing and dramatically reduced intermolecular interactions between the SFXSPO and TADF dyes. With assistance from the rigid configuration for structural relaxation suppression, a high T_1 value of 2.97 eV for positive energy transfer and favorable electrical performance, SFXSPO successfully realized state-of-the-art η_{ext} values up to 17.9%, 19.7%, 19.6%, 22.5%, 13.9%, and 19.0% and η_{int} of ≈100% for blue, green, yellowish green, yellow, orange, and complementary nearly white TADF diodes, respectively, manifesting SFXSPO as the best universal TADF host reported so far.

SFXSPO can be conveniently prepared from SFX through a successive two-step lithiation and phosphorylation reaction with a good yield of ≈60% (Figure 1a). Its chemical structure was fully characterized by NMR spectroscopy, mass spectroscopy, and elemental analysis. The configuration of SFXSPO was further confirmed by single-crystal X-ray diffraction (Figure 1a). As designed, the dihedral angle between the two phenyls of its xanthene is decreased to 155.6°, indicating the nonplanar structure with the spiro 9-C atom warped out. Consequently, fluorene in SFX tilts toward one side, significantly reducing the intersection angle between the fluorene and the xanthene to 72.6°. In contrast, with DPPO at the *para*-position, SFX in SFX2′PO[12c] is exactly orthogonal with a regular dihedral angle of xanthene of 173.6° and an intersection angle between fluorene and xanthene of ≈91° (Figure S1a, Supporting Information). Therefore, it is rational to attribute the highly twisted configuration of SFXSPO to the amplified steric bulk of its DPPO at the *ortho*-position. In consequence, even in single crystal, the molecular packing of SFXSPO is still locally disordered such that there are as many as six kinds of molecular orientations without any SFX-involved interactions observed (Figure 1b). On the contrary, the single-crystal packing diagram of SFX2′PO shows the π–π interactions between SFX cores with a centroid–centroid distance of 3.7 Å, ascribed to the regular molecular alignment with V only two different molecular orientations (Figure S1a, Supporting Information).

The formation of a twisted configuration through the *ortho*-linked DPPO gives rise to the enhanced molecular rigidity of SFXSPO, resulting in a high temperature of the glass transition (T_g) beyond 180 °C and melting point (T_m) approaching 280 °C, which indicates the strong morphological stability of SFXSPO (Figure S2, Supporting Information and **Table 1**). In spite of the big intramolecular tension, SFXSPO still reveals a good thermal stability with the temperature of decomposition (T_d) more than 300 °C and can be facilely evaporated in vacuo before 230 °C, making device fabrication feasible. The twisted rigid structure and highly disordered molecular alignment of SFXSPO make it easy to form amorphous thin films. The atom

Table 1. Physical properties of SFXSPO.

Compound	$\lambda_{Abs.}$ [nm]	$\lambda_{Em.}$ [nm]	η_{PL}[c] [%]	FWHM [nm]	S_1 [eV]	T_1 [eV]	RMS[h] [nm]	$T_g/T_m/T_d$ [°C]	HOMO [eV]	LUMO [eV]	μ_h/μ_e[k] [$cm^2 V^{-1} s^{-1}$]
SFXSPO	308, 279, 228[a]	311, 322[a]	23	24[a]	3.91[d]	2.97[g]	0.34	183/279/327		−2.47 (−2.31)[i]	8.98×10^{-7}
	309, 273, 231[b]	322[b]		24[b]	4.92[e]	2.98[e]			−6.52 (1.74)[i]	−2.61[j]	7.34×10^{-6}
					4.34[f]	3.15[f]			−6.09[e]	−1.17[e]	

[a]Absorption and emission in CH_2Cl_2 (10^{-6} mol L^{-1}); [b]Absorption and emission in film; [c]PLQY calculated by using 9,10-diphenylanthracene as standard; [d]Estimated according to the absorption edges; [e]DFT calculated results; [f]NTO calculated results; [g]Calculated according to the 0–0 transitions of the phosphorescence spectra; [h]Root-mean-square surface roughness of vacuum-evaporated film (100 nm); [i]Calculated according to the equation HOMO/LUMO = 4.78 + onset voltage; [j]Estimated according to the absorption bandgap and the HOMO energy level; [k]Hole and electron mobility evaluated by *I*–*V* characteristics of single carrier transporting devices with field-dependent space-charge-limited current model.

force microscopy (AFM) image of a vacuum-deposited film of SFXSPO (100 nm) shows a uniform and smooth surface with a root-mean-square (RMS) roughness of 0.34 nm (**Figure 2** and Table 1). Significantly, after doping with bis[4-(9,9-dimethyl-9,10-dihydroacridine)phenyl] sulfone (DMAC-DPS)[8] (10 wt%), 2,3,5,6-tetracarbazole-4-cyano-pyridine (4CzCNPy)[13] (5 wt%), 2,3,5,6-tetrakis(carbazol-9-yl)-1,4-dicyanobenzene (4CzTPN)[1b] (5 wt%), 3,4,5,6-tetrakis(3,6-diphenylcarbazol-9-yl)-1,2-dicyanobenzene (4CzPNPh)[1b] (5 wt%), and 2,3,5,6-tetrakis(3,6-diphenylcarbazol-9-yl)-1,4-dicyanobenzene (4CzTPNPh)[1b] (5 wt%) as blue, green, yellowish green, yellow, and orange TADF dyes, respectively, the coevaporated SFXSPO films preserved the smooth surface with almost unchanged RMS roughness around ≈0.3–0.4 nm, evidencing uniform dispersion of these TADF dyes in SFXSPO matrixes and their perfect compatibility (Figure 2 and Table S1, Supporting Information). In this sense, the aggregation and phase separation of the dopants were effectively suppressed by the rigid molecular structure and disordered molecular alignment of SFXSPO.

Density function theory (DFT) and time-dependent DFT calculations on the ground (S_0) state and the first singlet (S_1) and triplet (T_1) excited states of SFXSPO show that the SFX configurations of these three states approximately keep stable with similar intersection angles between fluorene and xanthene of 72.6°, 75.6°, and 78.1°, which is beneficial to suppress structural-relaxation-induced exciton quenching (Figure S3, Supporting Information). The singlet and triplet transition characteristics of SFXSPO were investigated with natural transition orbitals (NTO).[14] For the $S_0 \rightarrow S_1$ excitation, the "hole" is mainly localized on the xanthene; while the "particle" is dispersed on the fluorene and the DPPO-linked phenyl of the xanthane, characteristic of a hybrid transition with the major part of a charge transfer (CT) excited state and the minor part of a locally excited (LE) state. The CT-dominant transition renders the low oscillator strength (f) of 0.0374, corresponding to the small transition probability of SFXSPO, which would facilitate host–dopant energy transfer and exciton confinement on emitting dopants during the EL process.[15] The situation for NTOs of $S_0 \rightarrow T_1$ excitation is different that both the "hole" and the "particle" are thoroughly localized on the fluorene with transition characteristics of the LE state, in accord with the spin-density distribution of the optimized T_1 state on fluorene (Figure S4, Supporting Information). The nonplanar xanthene with reduced conjugation induces the T_1 state to concentrate on fluorene, giving rise to a high calculated T_1 energy of 2.98 eV for positive energy transfer to blue TADF dyes, such as DMAC-DPS (T_1 = 2.91 eV).

The electronic absorption spectrum of SFXSPO in dilute solution (10^{-6} in CH_2Cl_2) consists of three bands around 308, 279, and 228 nm, corresponding to the $n \rightarrow \pi^*$ transition from xanthene to fluorene, mixed $\pi \rightarrow \pi^*$ transitions of xanthene and fluorene, and $\pi \rightarrow \pi^*$ transition of DPPO, respectively (**Figure 3**a). In dilute solution (10^{-6} in CH_2Cl_2), SFXSPO reveals two fluorescence (FL) peaks at 310 and 322 nm, corresponding to 0→0 and 0→1 radiative transitions, respectively

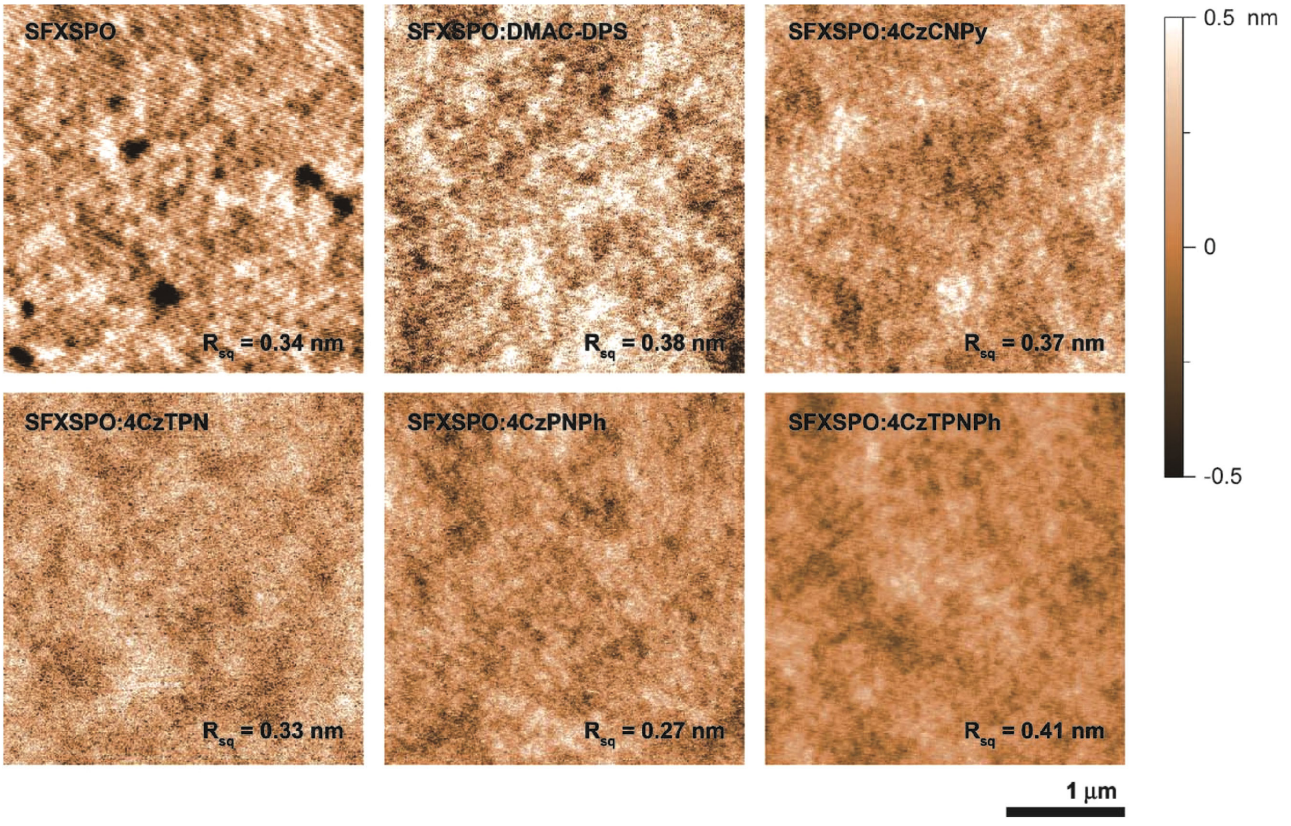

Figure 2. AFM images of vacuum-evaporated neat and TADF dyes-doped SFXSPO thin films with thickness of 100 nm (testing area: 3 μm × 3 μm). Doping concentrations were 10 wt% for DMAC-DPS and 5 wt% for 4CzCNPy, 4CzTPN, 4CzPNPh, and 4CzTPNPh, respectively.

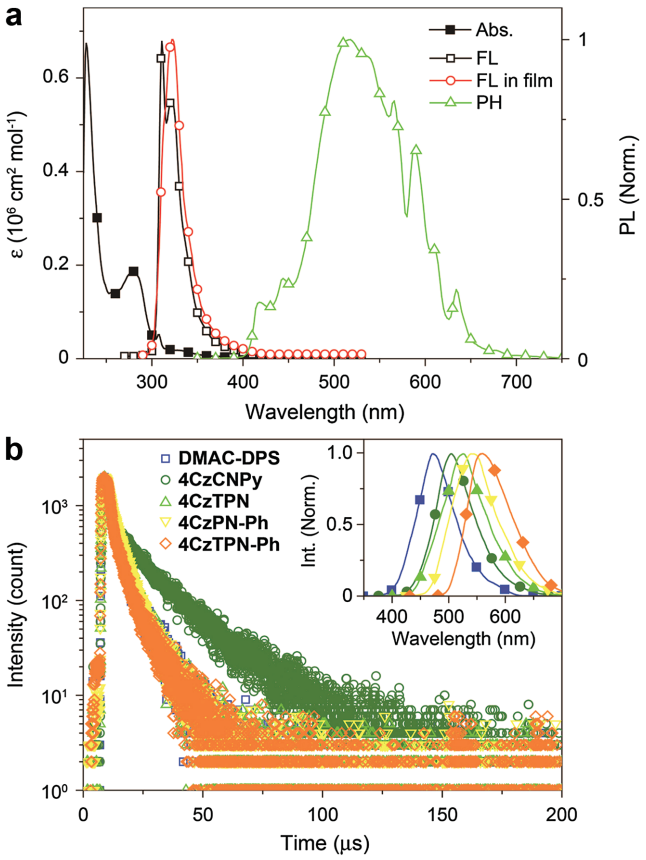

Figure 3. a) Electronic absorption, fluorescence (FL) in dilute solution (10^{-6} mol L^{-1}), FL in film and phosphorescence (PH) spectra of SFXSPO; b) time decay curves and emission spectra (inset) of vacuum-evaporated TADF dyes doped SFXSPO films (100 nm). DMAC-DPS for blue, 4CzCNPy for green, 4CzTPN for yellowish green, 4CzPNPh for yellow, and 4CzTPNPh for orange.

(Figure 3a). The relative photoluminescence quantum yield (PLQY) (η_{PL}) of SFXSPO is as low as 23%, due to its reduced conjugation and CT-featured excited state transition (Table 1). In accord with almost same optimized SFX configurations in the S_0 and S_1 states, as shown by quantum simulation, the first peaks in the absorption and FL spectra of SFXSPO are basically overlapped with a negligible Stokes shift of 21 cm^{-1}, manifesting an extremely suppressed excited-state structural relaxation. A single fluorescence peak at 322 nm from 0→1 transition is recognized in the emission spectrum of SFXSPO film. The absence of the peak originating from the 0→0 transition should be attributed to the restrained molecular vibration in solid state. From solution to film, the ignorable emission bathochromic shift further verifies the suppressed intermolecular aggregation and π–π interactions in the solid state by the distorted and asymmetrical configuration and disordered molecular packing of SFXSPO. Furthermore, with the full width at half maximum (FWHM) as small as 24 nm (Table 1), SFXSPO possesses fluorescent emissions even narrower than those of condensed aromatics, e.g., perylene with FWHM of ≈35 nm, ascribed to the limited transition processes due to its highly rigid structure. The phosphorescence spectrum was measured with time-resolved technology to get rid of the interferences from FL (Figure 3a). According to the first peak at 418 nm from 0→0 transition, the T_1 energy of SFXSPO is evaluated as 2.97 eV, identical to the DFT-calculated value, which can support the positive triplet energy transfer to full-color TADF dyes.

SFXSPO films doped with DMAC-DPS (10 wt%), 4CzCNPy (5 wt%), 4CzTPN (5 wt%), 4CzPNPh (5 wt%), and 4CzTPNPh (5 wt%), respectively, were prepared through vacuum evaporation (Figure 3b, and Figure S5 and Table S1, Supporting Information). The emissions from all of these films are thoroughly originated from their dopants, manifesting efficient host–dopant energy transfer. The absolute η_{PL} values of these films are as high as 83%, 95%, 99%, 100%, and 76% for DMAC-DPS, 4CzCNPy, 4CzTPN, 4CzPNPh, and 4CzPNTPh, accompanied with delayed fluorescence lifetimes (τ_{DF}) of 6.4, 14.2, 5.3, 5.1, and 5.1 μs, respectively. Except for 4CzCNPy, τ less than 10 μs of these TADF dyes in SFXSPO matrix is beneficial to suppress the triplet-involved quenching effects.

The carrier-injection ability of SFXSPO was investigated with cyclic voltammetry (Figure S6a, Supporting Information). SFXSPO shows one quasi-reversible anodic peak and one quasi-reversible cathodic peak at 2.53 and −2.93 V, corresponding to fluorene-attributed oxidation and reduction, respectively. According to the redox onsets, the experimental values of the highest occupied molecular orbital (HOMO) and the lowest unoccupied molecular orbital (LUMO) are −6.52 and −2.47 eV, which are almost equivalent to those of the spirofluorene-based analogue.[16] Therefore, in accordance to DFT calculation results (Figure S4, Supporting Information), the twisted and nonplanar xanthene in SFXSPO is hardly involved in the carrier-injection processes. In view of the LUMO and HOMO levels for electron- and hole-transporting layers around −2.7 and −5.2 eV, respectively, electron injection with a smaller barrier would be dominant in SFXSPO-based EMLs. The intrinsic carrier-transport performance of SFXSPO was evaluated by the current–voltage (I–V) characteristics of its nominal single-carrier transporting devices (Figure S6b, Supporting Information). SFXSPO displayed electron-dominant transportation with an electron-only current density (J) about one order of magnitude larger than the hole-only J. Estimated with the field-dependent space-charge-limited current model, the electron and hole mobility (μ_e and μ_h) of SFXSPO are appropriate as 7.34×10^{-6} and 8.98×10^{-7} cm^2 V^{-1} s^{-1}, respectively. Therefore, in spite of the highly disordered molecular packing, the intermolecular charge hoping in SFXSPO film can still be effective by virtue of the charge-transport network established by the pendent fluorene and DPPO.

In consequence, despite the distorted configuration and disordered molecular packing, SFXSPO still preserves the favorable electrical performance with major contributions from its fluorene and DPPO groups on the basis of its spirocyclic structure and short-axis linkage. The electron-predominant characteristics of SFXSPO can improve the charge flux balance in hole-redundant organic light-emitting diodes (OLEDs) employing conventional carrier transporting materials.

Encouraged by the well-controlled intermolecular interactions and favorable optoelectronic properties, SFXSPO was utilized to fabricate full-color TADF devices with DMAC-DPS, 4CzCNPy, 4CzTPN, 4CzPNPh, and 4CzPNTPh as blue, green, yellowish green, yellow, and orange TADF dopants, respectively,

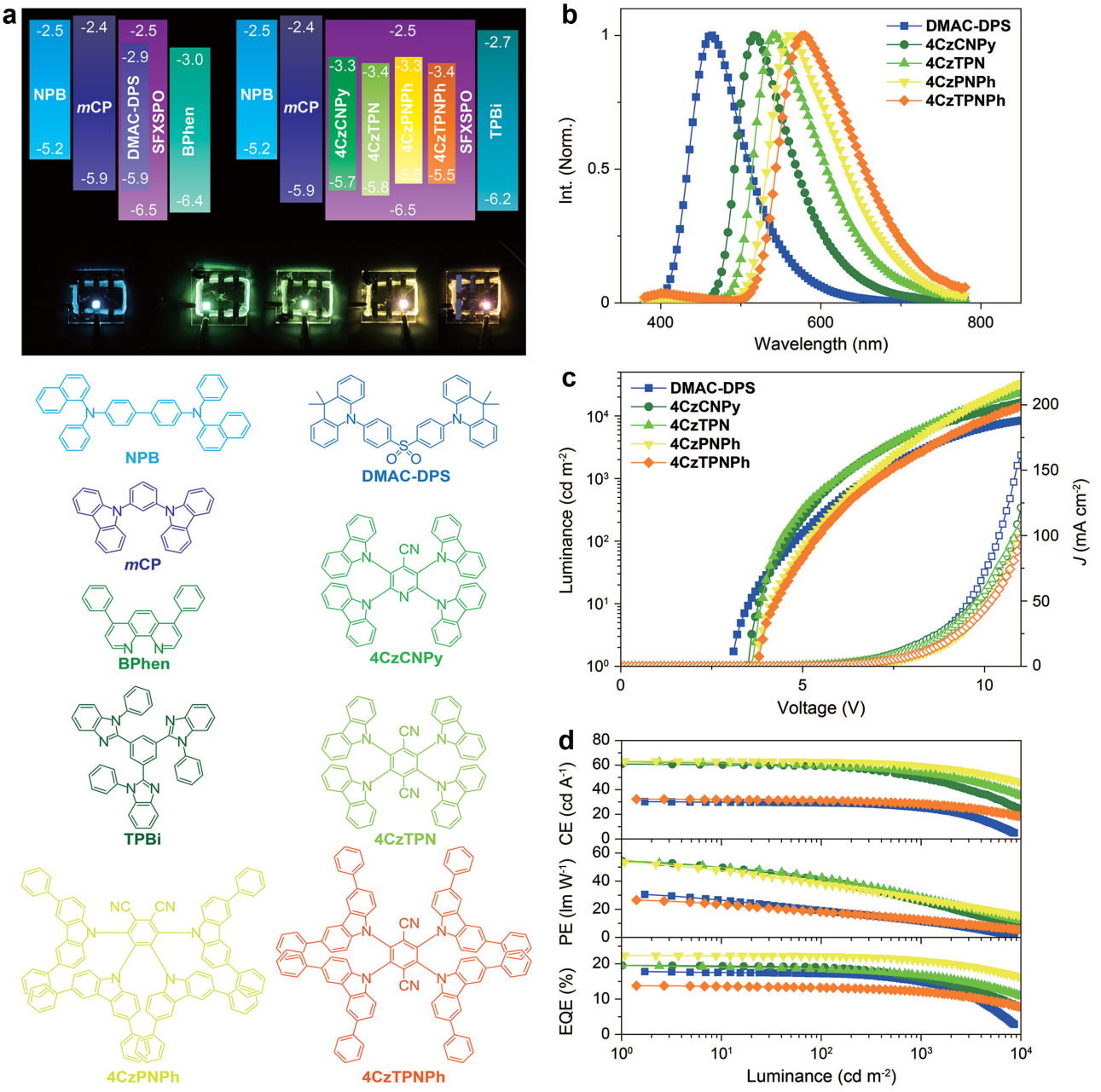

Figure 4. EL performance of blue, green, yellowish green, yellow, and orange TADF devices using SFXSPO as host. a) Device structures, energy level diagrams (left for blue; right for green, yellowish green, yellow, and orange), photos and chemical structures of employed materials; b) EL spectrum; c) luminance–current-density (*J*)–voltage curves; d) efficiency–luminance curves.

to verify its potential as universal TADF host (**Figure 4**a). To remedy the inferiority of DMAC-DPS in charge capture and stability, the doping concentration of the blue devices was optimized as 10 wt% (Figure S7, Supporting Information), accompanied by the employment of 4,7-diphenyl-1,10-phenanthroline (Bphen) with higher electron mobility and the deeper LUMO for charge flux balance (Figure S8, Supporting Information). Pure TADF dye-originated EL emissions were achieved with peaks at 464, 516, 540, 560, and 580 nm and favorable Commission Internationale de l'Éclairage (CIE) coordinates of (0.17, 0.20), (0.31, 0.59), (0.41, 0.56), (0.48, 0.51), and (0.52, 0.46), respectively, manifesting complete energy transfer from SFXSPO to these TADF dyes (Figure 4b). It is interesting that the EL spectra were identical to the PL spectra of these TADF dyes in toluene solution, which should be attributed to the uniform and neutral environment provided by the SFXSPO matrix.

The blue devices achieved low driving voltages of 3.0, ≈4.5 and ≈6.5 V for the onset and at 100 and 1000 cd m^{-2}, respectively (Figure 4c and Table S2, Supporting Information), ascribed to the barrier-free carrier injection through the HOMO and LUMO energy levels of DMAC-DPS equivalent to the corresponding molecular orbital energy levels of

N,N′-dicarbazole-3,5-benzene (*m*CP) and Bphen (Figure 4a). In this case, the direct carrier capture and exciton recombination on DMAC-DPS would be the main EL mechanism, with assistance from the host–dopant energy transfer at high driving voltages. In contrast, although the carrier-injection abilities of 4CzCNPy, 4CzTPN, 4CzPNPh, and 4CzPNTPh are stronger with the shallower HOMOs and the deeper LUMOs, SFXSPO would be simultaneously involved in electron injection, owing to its LUMO energy level comparable to that of 1,3,5-tri(1-phenyl-benzimidazole-2-yl)phenyl (TPBi), which makes the EL mechanism of host–dopant energy transfer considerable. In consequence, the green, yellowish green, yellow, and orange devices showed the higher onset voltages of 3.5–3.8 V, in coincidence with the triplet energy gaps between SFXSPO and these TADF dopants.

The maximum efficiencies of 30.3 cd A^{-1} for current efficiency, 30.7 lm W^{-1} for power efficiency, and 17.9% for η_{ext} were respectively achieved by the blue devices, accompanied with EQE roll-offs as 3% and 17% at 100 and 1000 cd m^{-2} comparable to the lowest values reported so far (Figure 4d and Table S2, Supporting Information).[17] The green devices displayed state-of-the-art efficiencies up to 60.9 cd A^{-1}, 54.6 lm W^{-1}, and 19.7%, but their EQE roll-off as 19% at 1000 cd m^{-2} was the most serious among these monocolor devices, which revealed the worst triplet exciton quenching due to the longest τ_{DF} of 4CzCNPy among these TADF dyes. It is rational that with the shorter τ_{DF}, 4CzTPN rendered the reduced EQE roll-off as 14% at 1000 cd m^{-2} for its yellowish green devices with the maximum efficiencies equivalent to those of the green analogues. Inspiringly, SFXSPO endowed its yellow devices with the record efficiencies as high as 63.3 cd A^{-1}, 53.7 lm W^{-1}, and 22.5%, accompanied by excellent efficiency stability with negligible EQE roll-offs of 1% and 7% at 100 and 1000 cd m^{-2}, respectively, verifying SFXSPO as the most efficient yellow TADF host to the best of our knowledge.[1c] Its orange devices also realized the high efficiencies of 32.4 cd A^{-1}, 26.8 lm W^{-1}, and 13.9%, and reduced EQE roll-offs of 4% and 12% at 100 and 1000 cd m^{-2}, respectively, which were remarkably improved in comparison to 4,4′-bis(*N*-carbazolyl)-1,1′-biphenyl-based analogues.[1b] Significantly, according to the relational expression:[18]

$$\eta_{ext} = \eta_{int} \cdot \eta_{OC} = \gamma \cdot \chi \cdot \eta_{PL} \cdot \eta_{OC} \quad (1)$$

in which η_{oc} refers to light out-coupling efficiency, regarded as a constant of 0.20 for indium tin oxide (ITO) glass substrate without any additional out-coupling enhancement, γ stands for hole–electron recombination efficiency given 1 when carrier flux balance and χ is radiative exciton fraction related to spin selection rule of 25% for singlet and 75% for triplet, η_{int} of SFXSPO-based devices were evaluated as high as 89.5%, 98.5%, 98.0%, 112.5%, and 69.5% for blue, green, yellowish green, yellow, and orange, respectively. Meanwhile, their χ values reached to 108%, 104%, 99%, 113%, and 91%, respectively, manifesting ≈100% utilization of both singlet and triplet exciton.

Table S2 (Supporting Information) lists the representative results of monocolor TADF diodes, in comparison to which SFXSPO displays comparable or dramatically improved device performance, testifying SFXSPO as the best universal TADF host to date.

The state-of-the-art performance of the SFXSPO-based monocolor TADF devices motivated us to demonstrate the first example of the efficient single-host-based full-TADF complementary nearly white OLEDs (WOLED) using DMAC-DPS and 4CzPNPh as blue and yellow emitters (Scheme S1, Supporting Information). Dual-peak emission was achieved with CIE coordinates of (0.32, 0.43) at 500 cd m^{-2} (inset in **Figure 5**a). Due to the thicker device structure, the driving voltages of these devices were slightly higher than those of blue and yellow analogues (Figure 5a and Table S2, Supporting Information). Significantly, state-of-the-art efficiencies were realized with maxima of 50.5 cd A^{-1}, 40.6 lm W^{-1}, and 19.1%, corresponding to a η_{int} as high as 95.5%, which are the record values of full-TADF WOLEDs[19] and comparable to full-phosphorescence[9a,11r,20] and TADF-phosphorescence hybrid WOLEDs[21] (Figure 5b and Table S2, Supporting Information). Nevertheless, these devices still suffered the EQE roll-offs of 4% and 18% at 100 and 1000 cd m^{-2}, respectively, which were about two folds of those of the yellow devices but approximate to those of the blue analogues. Furthermore, the intensity of blue component in their spectra was gradually decreased along with voltage increasing, making the emission shift to yellow zone (Figure 5c and Figure S9, Supporting Information). Through multipeak fitting analysis, the contributions of blue and yellow components to η_{ext} of white emission can be roughly evaluated by:[22]

$$\eta_{ext}^{C} = \eta_{ext} \times \frac{A^{C}}{A^{B} + A^{Y}} \quad (2)$$

in which superscript C can be B or Y referring to blue and yellow components, respectively, and A stands for peak area (Figure 5d). It is showed that η_{ext} of yellow component was only slight decreased from ≈10.5% to 9.5%, in contrast to the remarkable EQE reduction of blue component. Therefore, the considerable EQE roll-offs and unstable EL spectra of these devices should be assigned to rapid efficiency decrease of their blue-emitting units at high luminance. In this sense, the employment of highly efficient and stable blue TADF dyes can further improve the efficiency and spectral stability of SFXSPO-based full-TADF WOLEDs. To figure out the emission mechanism of the nearly white OLEDs, control devices with reversed blue and yellow EMLs were fabricated, which revealed stable pure yellow light from 4CzPNPh along with increasing voltage (Figure S10, Supporting Information). Accordingly, excitons should be first formed in blue EMLs of the nearly white OLEDs, and then partially transferred to yellow EMLs to generate the nearly white emissions. Considering the Dexter energy transfer distance and their yellow-dominant emissions, the recombination zones of these nearly white OLEDs should be close to the interface of two EMLs and keep stable during voltage variation.

As D–A systems featured with CT excited states and ambipolar characteristics, most TADF dyes are superior in charge flux balance and exciton recombination. In the case of heavy doping devices, actually, carrier injection and transportation can be basically supported by TADF dopants rather than host matrixes. The primary function of the TADF hosts is more embodied in uniformly dispersing dopants and suppressing quenching effects induced by dopant–dopant and host–dopant interactions. On account of the much shorter lifetime for

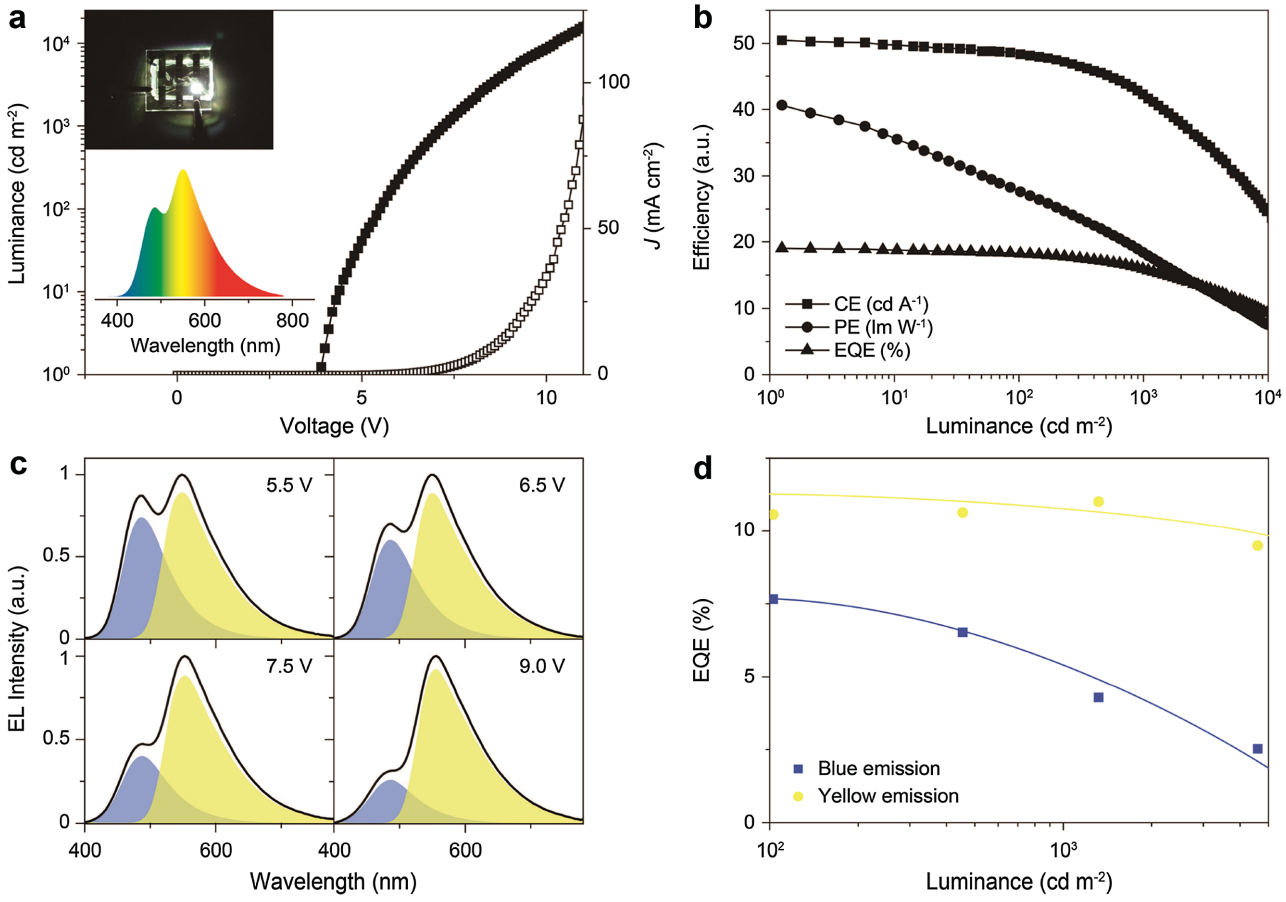

Figure 5. EL performance of full-TADF complementary nearly white diodes employing SFXSPO as a single host. a) Luminance–*J*–voltage curves and EL spectrum and device photo at 500 cd m^{-2} (inset); b) efficiencies versus luminance relationship; c) EL spectra at different driving voltages; d) variation tendency of EQE contributions from blue and yellow emission parts along with luminance increasing.

singlet excitons, STA requires more effective intermolecular collisions in contrast to TTA. It is noteworthy that the EQE decrease tendency of SFXSPO-based devices basically fitted with the TTA model[23] with small deviations, manifesting the significantly reduced STA (Figure S11, Supporting Information), which was remarkably different from other host materials based TADF devices.[4,24] In this sense, the great success of SFXSPO in full-color TADF diodes were doubtlessly attributed to its highly distorted configuration and disordered intermolecular packing.

In summary, a novel spirocyclic phosphine oxide host SFXSPO was constructed on the basis of a short-axis linkage strategy. The amplified steric bulk of its DPPO at the *ortho*-position effectively distorts the SFX core, giving rise to the nonplanar xanthene and oblique fluorene. The extremely twisted, rigid, and asymmetric conformation of SFXSPO renders the highly disordered molecular packing in its solid states, effectively mitigating intermolecular interactions and facilitating uniform dispersion of the TADF dyes in its amorphous films. With the superiority in effectively suppressing the quenching effects induced by structural relaxation and dopant–dopant and host–dopant interactions, SFXSPO successfully provided state-of-the-art performance to its full-color devices, e.g., the record η_{ext} of 22.5% and 19.1% and η_{int} of ≈100% for its yellow TADF diodes and single-host full-TADF complementary nearly white devices, respectively, manifesting SFXSPO as the best universal TADF host reported so far. Nevertheless, the efficiency stability of its blue and nearly white TADF diodes, as well as spectral stability of its WOLEDs, can be further improved when more efficient and stable blue TADF dyes are available, which leaves the space for further device optimization.

Supporting Information

Supporting Information is available from the Wiley Online Library or from the author.

Acknowledgements

J.L. and D.D. contributed equally to this work. This project was financially supported by the NSFC (Grant Nos. 61176020 and 51373050), New Century Excellent Talents Supporting Program of MOE (NCET-12-0706), Program for Innovative Research Team in University (MOE) (IRT-1237), Science and Technology Bureau of Heilongjiang Province (Grant Nos. ZD201402 and JC2015002), Education Bureau of Heilongjiang Province (Grant No. 2014CJHB005), the Fok Ying-Tong Education Foundation for Young Teachers in the Higher Education Institutions of China

(141012) and the Harbin Science and Technology Bureau (Grant No. 2015RAYXJ008).

Received: December 17, 2015
Revised: January 25, 2016
Published online: February 29, 2016

[1] a) A. Endo, M. Ogasawara, A. Takahashi, D. Yokoyama, Y. Kato, C. Adachi, *Adv. Mater.* **2009**, *21*, 4802; b) H. Uoyama, K. Goushi, K. Shizu, H. Nomura, C. Adachi, *Nature* **2012**, *492*, 234; c) Y. Tao, K. Yuan, T. Chen, P. Xu, H. Li, R. Chen, C. Zheng, L. Zhang, W. Huang, *Adv. Mater.* **2014**, *26*, 7931; d) H. Nakanotani, T. Higuchi, T. Furukawa, K. Masui, K. Morimoto, M. Numata, H. Tanaka, Y. Sagara, T. Yasuda, C. Adachi, *Nat. Commun.* **2014**, *5*, 4016.

[2] a) W. Li, D. Liu, F. Shen, D. Ma, Z. Wang, T. Feng, Y. Xu, B. Yang, Y. Ma, *Adv. Funct. Mater.* **2012**, *22*, 2797; b) H. Tanaka, K. Shizu, H. Nakanotani, C. Adachi, *Chem. Mater.* **2013**, *25*, 3766; c) Y.-S. Park, K.-H. Kim, J.-J. Kim, *Appl. Phys. Lett.* **2013**, *102*, 153306; d) X.-L. Chen, R. Yu, Q.-K. Zhang, L.-J. Zhou, X.-Y. Wu, Q. Zhang, C.-Z. Lu, *Chem. Mater.* **2013**, *25*, 3910.

[3] a) Q. M. Peng, W. J. Li, S. T. Zhang, P. Chen, F. Li, Y. G. Ma, *Adv. Opt. Mater.* **2013**, *1*, 362; b) B. Milián-Medina, J. Gierschner, *Org. Electron.* **2012**, *13*, 985; c) S. Huang, Q. Zhang, Y. Shiota, T. Nakagawa, K. Kuwabara, K. Yoshizawa, C. Adachi, *J. Chem. Theory Comput.* **2013**, *9*, 3872.

[4] K. Masui, H. Nakanotani, C. Adachi, *Org. Electron.* **2013**, *14*, 2721.

[5] G. Méhes, K. Goushi, W. J. Potscavage, Jr, C. Adachi, *Org. Electron.* **2014**, *15*, 2027.

[6] a) H. Zamani Siboni, H. Aziz, *Org. Electron.* **2013**, *14*, 2510; b) D. Song, S. Zhao, Y. Luo, H. Aziz, *Appl. Phys. Lett.* **2010**, *97*, 243304; c) C. Han, L. Zhu, J. Li, F. Zhao, Z. Zhang, H. Xu, Z. Deng, D. Ma, P. Yan, *Adv. Mater.* **2014**, *26*, 7070.

[7] a) V. Jankus, P. Data, D. Graves, C. McGuinness, J. Santos, M. R. Bryce, F. B. Dias, A. P. Monkman, *Adv. Funct. Mater.* **2014**, *24*, 6178; b) B. S. Kim, J. Y. Lee, *Adv. Funct. Mater.* **2014**, *24*, 3970; c) Y. J. Cho, K. S. Yook, J. Y. Lee, *Adv. Mater.* **2014**, *26*, 4050.

[8] a) H. Wang, L. Xie, Q. Peng, L. Meng, Y. Wang, Y. Yi, P. Wang, *Adv. Mater.* **2014**, *26*, 5198; b) J.-Y. Hu, Y.-J. Pu, F. Satoh, S. Kawata, H. Katagiri, H. Sasabe, J. Kido, *Adv. Funct. Mater.* **2014**, *24*, 2064; c) C. Mayr, S. Y. Lee, T. D. Schmidt, T. Yasuda, C. Adachi, W. Brütting, *Adv. Funct. Mater.* **2014**, *24*, 5232; d) M. Kim, S. K. Jeon, S.-H. Hwang, J. Y. Lee, *Adv. Mater.* **2015**, *27*, 2515; e) D. R. Lee, M. Kim, S. K. Jeon, S.-H. Hwang, C. W. Lee, J. Y. Lee, *Adv. Mater.* **2015**, *27*, 5861; f) Q. Zhang, D. Tsang, H. Kuwabara, Y. Hatae, B. Li, T. Takahashi, S. Y. Lee, T. Yasuda, C. Adachi, *Adv. Mater.* **2015**, *27*, 2096; g) T. Hofbeck, U. Monkowius, H. Yersin, *J. Am. Chem. Soc.* **2015**, *137*, 399; h) S. Hirata, Y. Sakai, K. Masui, H. Tanaka, S. Y. Lee, H. Nomura, N. Nakamura, M. Yasumatsu, H. Nakanotani, Q. Zhang, K. Shizu, H. Miyazaki, C. Adachi, *Nat. Mater.* **2015**, *14*, 330; i) Q. Zhang, B. Li, S. Huang, H. Nomura, H. Tanaka, C. Adachi, *Nat. Photonics* **2014**, *8*, 326; j) D. Graves, V. Jankus, F. B. Dias, A. Monkman, *Adv. Funct. Mater.* **2014**, *24*, 2343; k) X.-K. Liu, Z. Chen, C.-J. Zheng, C.-L. Liu, C.-S. Lee, F. Li, X.-M. Ou, X.-H. Zhang, *Adv. Mater.* **2015**, *27*, 2378; l) J. W. Sun, J. H. Lee, C. K. Moon, K. H. Kim, H. Shin, J. J. Kim, *Adv. Mater.* **2014**, *26*, 5684; m) Z.-Q. Zhu, T. Fleetham, E. Turner, J. Li, *Adv. Mater.* **2015**, *27*, 2533; n) D. Zhang, L. Duan, C. Li, Y. Li, H. Li, D. Zhang, Y. Qiu, *Adv. Mater.* **2014**, *26*, 5050.

[9] a) C.-C. Lai, M.-J. Huang, H.-H. Chou, C.-Y. Liao, P. Rajamalli, C.-H. Cheng, *Adv. Funct. Mater.* **2015**, *25*, 5548; b) E. Mondal, W.-Y. Hung, H.-C. Dai, K.-T. Wong, *Adv. Funct. Mater.* **2013**, *23*, 3096; c) H.-H. Chou, C.-H. Cheng, *Adv. Mater* **2010**, *22*, 2468.

[10] a) J. Kalinowski, W. Stampor, J. Mecedilzdotyk, M. Cocchi, D. Virgili, V. Fattori, P. Di Marco, *Phys. Rev. B* **2002**, *66*, 235321; b) S. Reineke, K. Walzer, K. Leo, *Phys. Rev. B* **2007**, *75*, 125328; c) Q. Wang, I. W. H. Oswald, M. R. Perez, H. Jia, B. E. Gnade, M. A. Omary, *Adv. Funct. Mater.* **2013**, *23*, 5420.

[11] a) T. P. I. Saragi, T. Spehr, A. Siebert, T. Fuhrmann-Lieker, J. Salbeck, *Chem. Rev.* **2007**, *107*, 1011; b) H.-F. Chen, S.-J. Yang, Z.-H. Tsai, W.-Y. Hung, T.-C. Wang, K.-T. Wong, *J. Mater. Chem.* **2009**, *19*, 8112; c) S. O. Jeon, K. S. Yook, C. W. Joo, J. Y. Lee, *J. Mater. Chem.* **2009**, *19*, 5940; d) H. Choi, S. Paek, N. Lim, Y. H. Lee, M. K. Nazeeruddin, J. Ko, *Chem. Eur. J.* **2014**, *20*, 10894; e) G. E. Eperon, V. M. Burlakov, P. Docampo, A. Goriely, H. J. Snaith, *Adv. Funct. Mater.* **2014**, *24*, 151; f) J.-W. Lee, D.-J. Seol, A.-N. Cho, N.-G. Park, *Adv. Mater.* **2014**, *26*, 4991; g) O. Malinkiewicz, A. Yella, Y. H. Lee, G. M. Espallargas, M. Graetzel, M. K. Nazeeruddin, H. J. Bolink, *Nat. Photonics* **2014**, *8*, 128; h) M. Liu, M. B. Johnston, H. J. Snaith, *Nature* **2013**, *501*, 395; i) H. Nakanotani, S. Akiyama, D. Ohnishi, M. Moriwake, M. Yahiro, T. Yoshihara, S. Tobita, C. Adachi, *Adv. Funct. Mater.* **2007**, *17*, 2328; j) B. Chen, Y. Jiang, L. Chen, H. Nie, B. He, P. Lu, H. H. Y. Sung, I. D. Williams, H. S. Kwok, A. Qin, Z. Zhao, B. Z. Tang, *Chem. - Eur. J.* **2014**, *20*, 1931; k) S. Shao, Z. Ma, J. Ding, L. Wang, X. Jing, F. Wang, *Adv. Mater.* **2012**, *24*, 2009; l) L.-H. Xie, R. Zhu, Y. Qian, R.-R. Liu, S.-F. Chen, J. Lin, W. Huang, *J. Phys. Chem. Lett.* **2009**, *1*, 272; m) G. Méhes, H. Nomura, Q. Zhang, T. Nakagawa, C. Adachi, *Angew. Chem., Int. Ed.* **2012**, *51*, 11311; n) K. Nasu, T. Nakagawa, H. Nomura, C. J. Lin, C. H. Cheng, M. R. Tseng, T. Yasuda, C. Adachi, *Chem. Commun.* **2013**, *49*, 10385; o) K. S. Yook, S. E. Jang, S. O. Jeon, J. Y. Lee, *Adv. Mater.* **2010**, *22*, 4479; p) L.-S. Cui, Y.-M. Xie, Y.-K. Wang, C. Zhong, Y.-L. Deng, X.-Y. Liu, Z.-Q. Jiang, L.-S. Liao, *Adv. Mater.* **2015**, *27*, 4213; q) Y.-Y. Lyu, J. Kwak, W. S. Jeon, Y. Byun, H. S. Lee, D. Kim, C. Lee, K. Char, *Adv. Funct. Mater.* **2009**, *19*, 420; r) L. Ding, S.-C. Dong, Z.-Q. Jiang, H. Chen, L.-S. Liao, *Adv. Funct. Mater.* **2015**, *25*, 645; s) M. Romain, D. Tondelier, B. Geffroy, O. Jeannin, E. Jacques, J. Rault-Berthelot, C. Poriel, *Chem. Eur. J.* **2015**, *21*, 9426; t) J. Chen, C. Shi, Q. Fu, F. Zhao, Y. Hu, Y. Feng, D. Ma, *J. Mater. Chem.* **2012**, *22*, 5164; u) Z. Li, B. Jiao, Z. Wu, P. Liu, L. Ma, X. Lei, D. Wang, G. Zhou, H. Hu, X. Hou, *J. Mater. Chem. C* **2013**, *1*, 2183; v) Y. Liu, L.-S. Cui, X.-B. Shi, Q. Li, Z.-Q. Jiang, L.-S. Liao, *J. Mater. Chem. C* **2014**, *2*, 8736; w) H. W. Lin, S. Y. Ku, H. C. Su, C. W. Huang, Y. T. Lin, K. T. Wong, C. C. Wu, *Adv. Mater.* **2005**, *17*, 2489; x) H. Wen, Q. Huang, X.-F. Yang, H. Li, *Chem. Commun.* **2013**, *49*, 4956; y) H. Chen, Z.-Q. Jiang, C.-H. Gao, M.-F. Xu, S.-C. Dong, L.-S. Cui, S.-J. Ji, L.-S. Liao, *Chem. - Eur. J.* **2013**, *19*, 11791; z) N. Rehmann, D. Hertel, K. Meerholz, H. Becker, S. Heun, *Appl. Phys. Lett.* **2007**, *91*, 103507.

[12] a) D. Lin, M. Sun, Y. Wei, L. Xie, X. Zhang, W. Huang, *Chin. Sci. Bull.* **2015**, *60*, 1237; b) L.-H. Xie, F. Liu, C. Tang, X.-Y. Hou, Y.-R. Hua, Q.-L. Fan, W. Huang, *Org. Lett.* **2006**, *8*, 2787; c) J. Zhao, G.-H. Xie, C.-R. Yin, L.-H. Xie, C.-M. Han, R.-F. Chen, H. Xu, M.-D. Yi, Z.-P. Deng, S.-F. Chen, Y. Zhao, S.-Y. Liu, W. Huang, *Chem. Mater.* **2011**, *23*, 5331.

[13] C. Tang, T. Yang, X. Cao, Y. Tao, F. Wang, C. Zhong, Y. Qian, X. Zhang, W. Huang, *Adv. Opt. Mater.* **2015**, *3*, 786.

[14] R. L. Martin, *J. Chem. Phys.* **2003**, *118*, 4775.

[15] C. Han, F. Zhao, Z. Zhang, L. Zhu, H. Xu, J. Li, D. Ma, P. Yan, *Chem. Mater.* **2013**, *25*, 4966.

[16] S. O. Jeon, K. S. Yook, C. W. Joo, J. Y. Lee, *Appl. Phys. Lett.* **2009**, *94*, 013301.

[17] J. Zhang, D. Ding, Y. Wei, F. Han, H. Xu, W. Huang, *Adv. Mater.* **2016**, *28*, 479.

[18] D. Yu, F. Zhao, Z. Zhang, C. Han, H. Xu, J. Li, D. Ma, P. Yan, *Chem. Commun.* **2012**, *48*, 6157.

[19] a) W. Song, I. Lee, J. Y. Lee, *Adv. Mater.* **2015**, *27*, 4358; b) T. Higuchi, H. Nakanotani, C. Adachi, *Adv. Mater.* **2015**, *27*, 2019; c) S. Y. Lee, T. Yasuda, Y. S. Yang, Q. Zhang, C. Adachi, *Angew. Chem., Int. Ed.* **2014**, *53*, 6402.
[20] M. C. Gather, A. Köhnen, K. Meerholz, *Adv. Mater.* **2011**, *23*, 233.
[21] a) Y. J. Cho, K. S. Yook, J. Y. Lee, *Sci. Rep.* **2015**, *5*, 7859; b) D. Zhang, L. Duan, Y. Li, D. Zhang, Y. Qiu, *J. Mater. Chem. C* **2014**, *2*, 8191; c) C.-J. Zheng, J. Wang, J. Ye, M.-F. Lo, X.-K. Liu, M.-K. Fung, X.-H. Zhang, C.-S. Lee, *Adv. Mater.* **2013**, *25*, 2205.
[22] C. Adachi, M. A. Baldo, S. R. Forrest, *J. Appl. Phys.* **2000**, *87*, 8049.
[23] M. A. Baldo, C. Adachi, S. R. Forrest, *Phys. Rev. B* **2000**, *62*, 10967.
[24] T. Furukawa, H. Nakanotani, M. Inoue, C. Adachi, *Sci. Rep.* **2015**, *5*, 8429.